NICMOS Observations of Low-Redshift Quasar Host Galaxies[1]

K. K. McLeod
Whitin Observatory, Wellesley College, Wellesley, MA 02481; kmcleod@wellesley.edu

B. A. McLeod
Harvard-Smithsonian Center for Astrophysics, 60 Garden St., Cambridge, MA 02138;
bmcleod@cfa.harvard.edu

ABSTRACT

We have obtained Near-Infrared Camera and Multi-Object Spectrometer images of 16 radio quiet quasars observed as part of a project to investigate the "luminosity/host-mass limit." The limit results were presented in McLeod, Rieke, & Storrie-Lombardi (1999). In this paper, we present the images themselves, along with 1- and 2-dimensional analyses of the host galaxy properties. We find that our model-independent 1D technique is reliable for use on ground-based data at low redshifts; that many radio-quiet quasars live in deVaucouleurs-law hosts, although some of the techniques used to determine host type are questionable; that complex structure is found in many of the hosts, but that there are some hosts that are very smooth and symmetric; and that the nuclei radiate at $\sim 2-20\%$ of the Eddington rate based on the assumption that all galaxies have central black holes with a constant mass fraction of 0.6%. Despite targeting hard-to-resolve hosts, we have failed to find any that imply super-Eddington accretion rates.

Subject headings: galaxies:photometry—galaxies:active—infrared:galaxies—quasars: general

1. Introduction

Host galaxy studies got the opportunity for a real boost in February 1997 when the Near-Infrared Camera and Multi-Object Spectrometer (NICMOS) was installed on the Hubble Space Telescope (HST). NICMOS combines the superb spatial resolution of HST with the benefits that long wavelengths provide for imaging the redder hosts against the overwhelming glare of the bluer quasar nuclei. We have used NICMOS to image 16 radio quiet quasars as part of a project to investigate the "luminosity/host-mass limit," the results of which were presented in

[1]NOTE: this printout contains degraded figures. Full resolution images can be found in http://www.astro.wellesley.edu/kmcleod/mm.ps

McLeod, Rieke, & Storrie-Lombardi (1999; hereafter MRS). In this paper, we present the images themselves, along with 1- and 2-dimensional analyses of the host galaxy properties.

The sample, listed in Table 1, is composed of all 10 quasars from our "high-luminosity sample" (the 26 highest-luminosity PG quasars with $z < 0.3$; McLeod & Rieke 1994b) that had not been previously observed with HST. To this we added 6 luminous quasars out to $z = 0.4$ for which ground-based attempts to resolve a host galaxy had failed. All 16 objects are in the redshift range $0.13 < z < 0.40$ with an average $z = 0.25$.

We have used a zero point of 21.80 magnitudes in the Vega system for the F160W filter (Lehár et al. 2000), and refer to the resulting magnitudes simply as "H." We note that this is fainter by 0.31 mag than the value we used in MRS. For computing rest-frame properties of the hosts, we assume $H_0 = 80$ km s^{-1} Mpc^{-1}, $q_0 = 0$, $\Lambda_0 = 0$ throughout, but our results are not strongly sensitive to cosmology. For example, at $z = 0.4$, the difference in proper distance between $q_0 = 0$ and 1 is 10%. We also apply galaxy H-band k-corrections appropriate for star-forming galaxies, but note these amount to less than 0.1 magnitude for the redshifts in our sample. For the nuclei, we have used colors and k-corrections from Cristiani & Vio (1990). To compute $M_B(nuc)$, we have assumed that in the B-band all of the light belongs to the nucleus. This is a reasonable assumption for these high-luminosity quasars because (i) we know *ex post facto* that the galaxies are generally less luminous than the nuclei in the H-band, and (ii) the galaxy contribution relative to the nucleus falls dramatically at shorter wavelengths (see e.g. McLeod & Rieke 1995, Fig. 1).

2. NICMOS Observations

We observed each quasar in a single orbit with the NIC2 camera and the F160W filter (approximately the H band). A small amount of time at the end of each orbit was used to observe a star for characterizing the point-spread-function (PSF) of the telescope. These "PSF stars" were chosen within $2'$ of the quasar, which is the maximum allowed slew that does not require overhead for acquisition of new guide stars. For 11 quasars, we used our own ground-based H-band images to locate the infrared-brightest star within the $2'$ limit. For the remaining five quasars, we chose the visually brightest star from the Guide Star Catalog. These PSF stars do not have the same colors as the quasars, but this has not caused problems; we show below that the results are insensitive to PSF used.

All of the quasars and PSF stars were observed in MULTIACCUM mode, which records data in a series of increasingly long nondestructive readouts. The reduction software determines the average count rate for each pixel individually by fitting those parts of the integration ramps that are not saturated. This allows us to build up an image that is linear over the entire field, including on the bright quasar core. We can therefore avoid some of the difficulties previously encountered with PSF-subtraction in WFPC2 exposures, where the quasar core is necessarily saturated out to $\sim 0\farcs5$. The total on-source times for the quasars ranged from 1792 to 2304 sec, while the totals

Table 1. Results of 1D analysis[a]

Name	z	m_H (nuc)	M_H (nuc)	m_H (host)	M_H (host)[b]	M_B (nuc)[b]	F_{host}/F_{nuc}	L/L_{Edd}[c]
PG0026+129	0.142	13.3	-25.5	15.2	-23.6	-23.7	0.17	0.16
PG0947+396[d]	0.206	14.3	-25.3	15.4	-24.2	-23.1	0.37	0.05
PG1048+342	0.167	15.5	-23.7	15.1	-24.1	-23.2	1.48	0.07
PG1121+422[d]	0.224	14.6	-25.3	17.0[e]	-22.8[e]	-23.7	0.11	0.31[e]
PG1151+117	0.176	14.6	-24.7	15.9	-23.3	-23.6	0.29	0.19
PG1322+659	0.168	14.3	-24.9	15.6	-23.5	-23.2	0.29	0.10
PG1352+183	0.158	15.0	-24.0	15.1	-23.9	-23.2	0.92	0.07
PG1354+213	0.300	15.7	-24.9	16.1	-24.4	-24.6	0.73	0.16
PG1427+480[d]	0.221	15.0	-24.9	16.1	-23.7	-23.3	0.35	0.11
PG2233+134	0.325	15.2	-25.6	16.7	-24.0	-24.3	0.26	0.20
MARK876	0.129	13.6	-25.0	13.3	-25.3	-23.0	1.36	0.02
UM357	0.334	15.1	-25.8	16.7	-24.0	-24.2	0.22	0.17
Q0530-379	0.334	15.5	-25.4	16.9	-23.9	-23.4	0.28	0.09
NAB1612+26	0.395	15.6	-25.6	17.3	-23.9	-23.4	0.22	0.10
1628.6+3806[d]	0.394	15.2	-26.0	16.7	-24.4	-23.7	0.26	0.08
KUV18217+6419[d]	0.297	12.3	-28.2	14.7	-25.7	-26.0	0.11	0.20

[a] $H_0 = 80$ km s^{-1} Mpc^{-1}, $q_0 = 0$

[b] Includes k-correction.

[c] Using $M_B = M_H - 2.1 - 2.5[log_{10}(L/L_{edd}) + log_{10}(\frac{\Upsilon_V}{7.2 M_\odot/L_\odot}) + log_{10}(\frac{f}{0.006}) - log_{10}(\frac{BC}{12})]$ with $\Upsilon_V, f,$ and BC given by their default values (MRS)

[d] Used PSF0026 instead of quasar's own PSF star

[e] Detection is uncertain

for the PSF stars were 32-128 sec.

For most of the quasars, the MULTIACCUM sequences were obtained in a four-position SPIRAL-DITH pattern with a dither size of 1.″0875, corresponding to 14.5 NIC2 pixels. This offset was chosen to be large enough so that the quasar nucleus was on a different set of pixels on each of the four exposures, but small enough to provide a reliable half-pixel offset to improve the sampling of the otherwise slightly undersampled image. The dithering also allowed recovery of data lost due to cosmic rays. The PSF stars were observed in the same four-position SPIRAL-DITH, and all of the quasar and PSF dithers were centered on the same part of the chip (within $< 1''$). For four objects with extended hosts and/or large companions (PG0026+129, PG0947+396, PG1048+342, MRK876) we extended the area covered by observing in a 7 or 8 position SPIRAL-DITH-CHOP pattern, four positions of which coincided with the positions used for the rest of the objects.

3. Data Reduction

We reduced all of the quasar and PSF images using *nicred_1.8* , a set of C programs and IRAF[2] scripts developed for use with NICMOS images (B. McLeod 1997; Lehár et al. 2000). This version improves upon earlier versions of the pipeline and *nicred* by lowering the threshhold at which saturation is flagged. This is especially important for bright sources like our quasar cores, where significant charge can build up before the first readout.

The F160W flat and dark images are on-orbit exposures processed and provided by NICMOS Deputy PI M. Rieke. For the rest of the calibration we used the *nicred* files except that we modified the bad pixel mask to account for (i) the coronagraphic hole in the upper left portion of the images, and (ii) pixels that were obviously bad in many of our frames. In addition, cosmic ray hits were flagged by hand for each image as part of the *nicred* reduction process.

The resulting images from each dither position were magnified by a factor of 2 and then aligned and combined to produce the final image for each object. The central 9.″6 of the 20″ reduced quasar images are shown in the first column of Fig. 1, and those of the PSFs are shown in Fig. 2. The final pixel scale is $\sim 0.''0375$. The PSF "star" selected for PG1121+422 turned out to be a compact galaxy and is not shown. For the quasar images, the 1σ scatter per pixel in blank sky corresponds to a limiting surface brightness of $H = 22.2$ mag arcsec^{-2} (or $V \approx 25.6$ mag arcsec^{-2} for a typical galaxy moved to the average redshift of our sample).

[2]IRAF (Image Reduction and Analysis Facility) is distributed by the National Optical Astronomy Observatories, which are operated by the Association of Universities for Research in Astronomy, Inc., under contract with the National Science Foundation.

4. One-Dimensional Analysis

4.1. Method

To estimate the magnitudes of the quasar host galaxies, we first performed a model-independent 1D removal of the nuclear point source for each object. This analysis differs somewhat from the technique used in MRS, and is better suited to the rereduced the data with the improved *nicred_1.8* saturation limits. The results here supersede those in the earlier paper. We assume that the H-band light from the quasar is composed of only two components: the host galaxy, which in the H-band is largely due to light from red giant stars; and the nucleus, taken to be a point source with image shape given by the PSF of the telescope. We do not assume a particular model for the galaxy, except to assume that its flux decreases monotonically away from its center.

We start by extracting from circular annuli 1D radial intensity profiles of the 16 quasars and the 15 PSF stars. The profile for the brightest PSF star, corresponding to PG0026+129 and called hereafter PSF0026, is shown in Fig. 3. We then scale the PSF profiles to have the same central flux as the quasar profile, and subtract from the quasar the highest PSF fraction that leaves a monotonic profile inside the first Airy minimum. Without assuming a particular functional form for the host galaxy radial profile, this "just monotonic" subtraction provides a reasonable estimate of the host flux (McLeod & Rieke 1994a). Finally, we numerically integrate the difference profiles, excluding any light from companions. We can typically integrate the profiles to a surface brightness of $H \approx 25.7$ mag arcsec^{-2} (corresponding to $V \approx 29$ mag arcsec^{-2}). The resulting host galaxy magnitudes are given in Table 1, and the profiles are shown in Fig. 4.

In four cases where the quasar's own PSF was faint compared to the quasar, and in the case of PG1121+422 which has no PSF star, we have used PSF0026 for the analysis instead. To test the reliability of using another quasar's PSF, we repeated our analysis using PSF0026 on all of the objects. The resulting host magnitudes were acceptably close, with $<$ H(own psf) $-$ H(PSF0026) $>= 0.01 \pm 0.11$. This is an indication that the azimuthal average of the NIC2 PSF is relatively stable. In Figure 5, we plot the central parts all 15 PSF star profiles together, to show graphically the extent to which this is so.

4.2. Reliability

The assumption inherent in our 1D method is that the galaxy contributes little flux to the profile inside the first Airy minimum. The procedure we use is effectively equivalent to the one used with our ground-based data, where we subtracted just enough PSF to make the difference profile flatten out at the center. We can now use NICMOS data to test the effect of seeing on this procedure for the ground-based data, by comparing the magnitudes for the 8 quasars where we have ground-based detections (McLeod & Rieke 1994b). We find the average value of $<$ H(HST) $-$ H(ground) $>= 0.08 \pm 0.27$, which is in good agreement with the 0.30 mag uncertainty

quoted for our ground-based data (McLeod & Rieke 1994b). One of the most discrepant points is due the presence of a companion that could not be resolved from the ground. We conclude that, despite an order-of-magnitude difference in resolution, the ground-based host magnitudes derived by this method for low-redshift quasars are fairly robust when nearby companions can be resolved.

Our 1D analysis is simplistic but has the advantage of not assuming *a priori* a model for the host galaxy. The amount by which our technique underestimates the host flux is dependent on the exact profile of the galaxy. To understand the limitations of this method, we generated a grid of model quasar images covering a range of type (deVaucouleurs and exponential), effective radius and scale length (0.5-1″, corresponding to 1.5-3 kpc for the average redshift of our sample), and total host intensity relative to the nucleus (1-30%, corresponding to galaxies in the range 13-16.7 mag). We modeled the quasar as point source + galaxy, and convolved the image with one our observed PSF stars. We then ran our 1D analysis technique on the images using PSF0026 as the "PSF star." We find that for all the model galaxies with $> 1\%$ of the nuclear luminosity, this technique underestimates the true host flux by $\lesssim 0.2$ mag. For the galaxies at 1%, errors in estimating the background level for the profile dominate the procedure, and the resulting host magnitude errors can be much higher, up to 0.7 mag off in either direction. For the real quasars in our sample, the 1D analysis yielded hosts with total luminosity from 10-150% of the nuclear luminosity. Only one host, that of PG1121+422, is at both a low fraction (11%) and at the faint end where background errors are worrisome. Therefore, we treat its detection and magnitude as uncertain, but estimate that the rest of the host magnitudes have an accuracy of ~ 0.2 mag.

4.3. Results

In Fig. 4, each quasar profile is shown plotted versus both linear radius r and $r^{1/4}$. These plots can be used to judge how well the profiles approximate an exponential disk law (straight line on the plots versus r) or deVaucouleurs law (straight line on the plots versus $r^{1/4}$). One can see from this Figure that the shape of the galaxy's profile outside the central 0.″4 is very little affected by even large errors in PSF subtraction (compare the "just monotonic" and "100%" curves). Eyeball inspection of these plots shows that some of the profiles clearly follow a deVaucouleurs law, for example NAB1612+26 and KUV18217+6419. In some cases, the choice is dependent upon the PSF fraction subtracted. We now turn to a more complete analysis of host morphology using the full 2D information in the images.

5. Two-Dimensional Analysis

5.1. Method

To characterize the properties of the host galaxies using the full 2D information in the NICMOS images, we have fit the quasars with combinations of point sources, deVaucouleurs galaxies, and exponential disk galaxies, all convolved with a PSF image. The goodness-of-fit is determined by a merit that is the weighted sum of the squares of the residuals over all the pixels. We modeled each quasar using different combinations of the following components: (i) the background level (parametrized by a single number), (ii) the nucleus (intensity I_n, position x_n, y_n), and (iii) the host galaxy (I_g, x_g, y_g, position angle θ, axis ratio b/a, and scale length r_{eff} for a deVaucouleurs law or r_0 for an exponential disk). When other galaxies were present in the field, we fit those simultaneously to make sure their contributions would not bias the host galaxy parameters.

We performed many tests of the fitting procedure's robustness, finding that we could not always vary all the parameters simultaneously; in the case of tiny PSF mismatches, the fitting program would sometimes turn the "galaxy" component into a long, off-center, thin spike to match a high spatial frequency, high signal-to-noise PSF feature. We therefore constrained the galaxy and quasar to have the same position, i.e. we assumed the nucleus was in the center of the galaxy. In tests where we relaxed this assumption, and where the galaxy was not turned into a spike, the fitted positions of nucleus and host galaxy agreed within $0\farcs01$ (3σ), corresponding to 30pc at the distance of the average quasar.

We list in Tables 2 and 3 the galaxy parameters for the deVaucouleurs and exponential models from unweighted fits using each quasar's own PSF (χ^2 weighting is discussed in §5.3). The host galaxy magnitudes derived from the deVaucouleurs fits are in good agreement with the 1D method, with an average difference of $< \mathrm{H(deV)} - \mathrm{H(1D)} >= 0.07 \pm 0.27$. As is commonly seen in host profile fitting, the exponential fits give hosts systematically fainter than the 1D fits and deVaucouleurs fits by 0.7 mag, with a 1σ spread of 0.30 mag.

In the second column of Fig. 1, we show the quasars after removal of the nucleus based on 2D deVaucouleurs fits using the high signal-to-noise PSF0026 (at this stretch, the ones based on 2D exponential fits are visually indistinguishable). We also show in Fig. 1 the residuals after subtracting both the nucleus and the model galaxy for both types of host. The fitting technique has done a superb job of removing most of the complex features of the NICMOS PSF. It is immediately obvious that few of these hosts are perfectly fit by ideal deVaucouleurs and exponential models. However, subtracting out the smooth models does reveal interesting structure, which we discuss in §6. In general, structure can be believed outside of the central $0\farcs5$ diameter noisy region, and, in a few galaxies, the regions around the diffraction spike residuals.

Table 2. Results of 2D deVaucouleurs Fits[a]

ID	Own PSF			Best PSF							
	m_H (host)	r_{eff} ($''$)	b/a	m_H (nuc)	M_H (nuc)	m_H (host)	M_H (host)[b]	r_{eff} ($''$)	r_{eff} (kpc)[c]	b/a	PSF
PG0026+129	14.7	2.3	0.87	13.2	-25.6	14.7	-24.1	2.3	4.9	0.87	0026
PG0947+396	...	...	...	14.3	-25.4	14.9	-24.7	2.6	7.4	0.83	1821
PG1048+342	15.5	0.4	0.67	15.2	-24.0	15.4	-23.8	0.8	1.8	0.61	0026
PG1121+422	...	...	...	14.5	-25.4[d]	17.2[d]	-22.6[d]	3.9[d]	11.8[d]	0.92[d]	0026
PG1151+117	15.9	0.4	0.66	14.5	-24.8	15.7	-23.6	0.6	1.6	0.82	0026
PG1322+659	...	...	...	14.1	-25.0	15.8	-23.4	0.7	1.8	0.95	0026
PG1352+183	15.3	1.2	0.83	14.8	-24.3	15.2	-23.8	1.4	3.3	0.79	1821
PG1354+213	16.1	1.0	0.71	15.6	-25.0	16.2	-24.3	0.7	2.7	0.75	0026
PG1427+480	16.0	0.5	0.89	14.9	-24.9	16.0	-23.8	0.5	1.5	0.89	0026
PG2233+134	16.5	0.6	0.95	15.2	-25.6	16.7	-23.9	0.4	1.7	0.63	1821
MARK876	13.4	1.8	0.83	13.3	-25.3	13.0	-25.5	4.1	8.0	0.80	0026
UM357	17.1	1.3	0.54	14.9	-25.9	17.2	-23.5	1.3	5.0	0.43	0026
Q0530-379	17.3	0.2	0.71	15.3	-25.5	17.1	-23.6	0.7	2.7	0.71	0026
NAB1612+26	17.2	0.3	0.79	15.6	-25.6	17.2	-23.9	0.3	1.4	0.79	1612
1628.6+3806	16.7	0.2	0.67	15.1	-26.1	16.8	-24.4	0.6	2.6	0.73	0026
KUV18217+6419	...	...	...	12.3	-28.2	14.7	-25.7	0.3	1.1	0.87	1821[e]

[a] $H_0 = 80$ km s^{-1} Mpc^{-1}, $q_0 = 0$

[b] Includes k-correction

[c] Based on angular diameter distance, not an isophotal one

[d] Detection is uncertain

[e] From masked fit; no unmasked fits converged

Table 3. Results of 2D Exponential Fits[a]

ID	Own PSF			Best PSF							
	m_H (host)	r_0 ($''$)	b/a	m_H (nuc)	M_H (nuc)	m_H (host)	M_H (host)[b]	r_0 ($''$)	r_0 (kpc)[c]	b/a	PSF
PG0026+129	15.8	0.4	0.81	13.2	-25.6	15.8	-23.0	0.4	0.8	0.81	0026
PG0947+396	...	...	...	14.3	-25.4	15.9	-23.7	0.5	1.5	0.77	1821
PG1048+342	16.1	0.2	0.69	15.1	-24.0	16.0	-23.1	0.2	0.6	0.64	0026
PG1121+422	...	...	...	14.5	-25.4	18.0[d]	-21.8[d]	0.7[d]	2.0[d]	0.79[d]	0026
PG1151+117	16.3	0.2	0.81	14.5	-24.8	16.2	-23.0	0.2	0.6	0.90	0026
PG1322+659	...	...	...	14.1	-25.1	16.4	-22.8	0.2	0.6	0.92	0026
PG1352+183	16.0	0.3	0.87	14.7	-24.3	15.9	-23.1	0.4	0.9	0.89	0026
PG1354+213	16.8	0.3	0.80	15.5	-25.0	16.8	-23.7	0.2	0.9	0.81	0026
PG1427+480	16.5	0.2	0.91	14.9	-24.9	16.5	-23.3	0.2	0.5	0.91	0026
PG2233+134	17.1	0.2	0.95	15.1	-25.6	17.0	-23.6	0.3	1.0	0.94	0026
MARK876	14.5	0.4	0.88	13.3	-25.3	14.3	-24.2	0.5	1.0	0.87	0026
UM357	17.8	0.4	0.72	14.9	-25.9	17.8	-22.9	0.4	1.4	0.56	0026
Q0530-379	17.7	0.1	0.74	15.3	-25.5	17.7	-23.0	0.2	0.8	0.77	0026
NAB1612+26	17.7	0.2	0.74	15.5	-25.7	17.7	-23.4	0.3	1.1	0.60	0026
1628.6+3806	17.2	0.1	0.73	15.1	-26.1	17.2	-23.9	0.2	1.1	0.76	0026
KUV18217+6419	...	...	...	12.3	-28.3	15.3	-25.1	0.3	1.3	0.46	0026

[a] $H_0 = 80$ km s^{-1} Mpc^{-1}, $q_0 = 0$

[b] Includes k-correction

[c] Based on angular diameter distance, not an isophotal one

[d] Detection is uncertain

5.2. Reliability

To test the sensitivity of the fits to the properties of the PSF star and to possible sampling effects in the PSF cores, we repeated the deVaucouleurs and exponential fits for each quasar with the five PSF stars having the highest signal-to-noise, running each fit both with and without a mask that excluded the quasar nucleus inside a $0\farcs37$ diameter. Thus, we have fit each quasar $5 \times 2 \times 2 = 20$ different ways. We list in Tables 2 and 3 the results of the "best" fits, i.e. those using the PSF that gave the lowest merit for each quasar and galaxy type. This was often the high signal-to-noise PSF0026. We find that there are minor differences in the residuals around the first Airy ring, which can probably be attributed to telescope breathing. The effect on the photometry can be quantified by comparing the results of the "own" and "best" fits. We find that the host magnitude is robust for both deVaucouleurs and exponential fits, with $< \mathrm{H(own)} - \mathrm{H(best)} >_{\mathrm{deV}} = -0.04 \pm 0.18$ and $< \mathrm{H(own)} - \mathrm{H(best)} >_{\mathrm{exp}} = -0.04 \pm 0.08$ respectively. The radii for exponential fits generally agree within $0\farcs05$, corresponding to 0.15 kpc for a typical quasar in our sample. However, with a scatter of $0\farcs7$, the deVaucouleurs radii are found to be much less certain. This effect, seen also by McLure, Dunlop, & Kukula (1999; hereafter MDK), arises from a degeneracy whereby the fit can steal light from the nucleus to put into the peaky deVaucouleurs galaxy. For both types of galaxies, the axial ratios agree within $b/a \sim 0.1$. We find a nearly identical result when we compare the results from the normal fits to those where we mask out the central few pixels to avoid having the merit function dominated by noise in the bright centers.

As a further test of the 2D method, we explored the level to which our method might fabricate galaxies when none are detectable. To do this, we forced nucleus + galaxy fits to two true point sources, namely the bright PSFs corresponding to KUV18217+6419 and PG1151+117 (a PSF that is not as well matched to the others). We fitted them using the 5 PSFs used with the quasars and assuming both deVaucouleurs and exponential models for the "galaxies." Of these 20 combinations, the fits diverged to give negative or linear "galaxies" 18 times. The negative fluxes corresponded to a level only 0.4% that of the point source. In two cases with PG1151+117's PSF, the method fabricated an exponential disk with reasonable physical parameters. These "galaxies" have fluxes of only 12% and 2% that of the point source. Given the flux levels for our quasars, this test suggests that all the host detections are secure with the possible exception of PG1121+422 and KUV18217+6419, for which any exponential solutions must be treated as suspect.

Finally, the nuclear magnitudes from all of the fits appear extremely robust. We measure $< \mathrm{H(deV)} - \mathrm{H(exp)} >= 0.025 \pm 0.021$, $< \mathrm{H(deV)} - \mathrm{H(1D)} >= -0.13 \pm 0.10$, and $< \mathrm{H(exp)} - \mathrm{H(1D)} >= -0.15 \pm 0.09$ The three quasars with large differences (~ 0.3 mag) in nuclear magnitudes between the 1- and 2D fits are the ones in which the galaxy light constitutes $\gtrsim 0.5$ of the total in the H-band.

We conclude based on these tests that, for pure exponentials and deVaucouleurs hosts, the nuclear magnitudes and the host magnitudes, position angles, and exponential scale lengths are

robust within the uncertainties quoted above, but that the deVaucouleurs radii are less reliable.

5.3. χ^2 Weighting

Based on inspection of the residual images and the tests described above, we believe our unweighted fits give good estimates of the host parameters. However, the merit function used does not provide a well-defined statistical discriminant between deVaucouleurs and exponential models for the hosts. Following the approach of MDK, we have attempted to assess the preference for one or the other type using a χ^2 analysis.

We first generated an azimuthally symmetric error map from each quasar image by masking out companions and assigning the error at each radius to be the standard deviation σ in circular annuli centered on the quasar. We then re-ran the fits with the $1/\sigma^2$ weight map and the high signal-to-noise PSF0026 (we found that the $1/\sigma^2$ weighting scheme fails with fainter PSFs where the fits become dominated by the noisy wings). As in MDK, maps of χ^2_ν generated by the PSF0026 fits are very uniform, so that no one area dominates the fitting. However, the fits generally resulted in overall χ^2 values less than the number of degrees of freedom, indicating that we have overestimated the size of the errors. This is because azimuthal structure in the PSF inflates the rms error around each annulus.

We have compared the resulting galaxy parameters to those generated by the best unweighted fits. Excluding PG1121+422, which is again suspect, and KUV18217+6419, for which no unweighted deVaucouleurs fit converged even though it is clearly an $r^{1/4}$ host based on the 1D profile, the host magnitudes and axial ratios have exactly the same spread as the uncertainties quoted above. The galaxy sizes, however, are significantly different. The weighted fits give systematically larger ellipticals and spirals by $0\farcs6$ (or 1.5 times) and $0\farcs3$ (or 1.9 times) respectively, with a large spread. One possible reason is that down-weighting the nuclear region allows less of the point-source component, which has a small scale length, to be attributed to the host.

6. Discussion

6.1. Host Galaxy Types

One of the most interesting results of quasar host galaxy research in the past few years has been the debunking of the textbook myth "radio-loud quasars live in ellipticals, radio-quiet quasars live in spirals." While early ground-based studies had shown this statement to be an oversimplification (Hutchings 1995), the improvement of instruments and the arrival of HST has made more detailed analyses possible. Various studies over the past few years, each including one to several dozen nearby quasars, have claimed that radio-quiet quasars often inhabit non-spiral hosts, and that the elliptical fraction likely increases with nuclear luminosity.

There have been many techniques used to assess the host type. McLeod & Rieke (1995) combined their ground-based near-IR host magnitudes with visual inspection of WFPC2 images from several groups to determine that there is a strong preference for high-luminosity quasars to have smooth, early-type hosts. Taylor et al. (1996) applied a 2D χ^2 modeling technique like that of MDK to their ground-based, near-IR images and found that almost half of the radio-quiet quasars lie in deVaucouleurs galaxies. Rönnback et al. (1996) applied a χ^2 test to 1D profiles to determine that the radio-quiet objects are found in both ellipticals and spirals; however, they performed the fits to profiles that had already had the PSF removed, the normalization of which can alter their results for reasons they outline. Bahcall et al. (1997) took advantage of the superior resolution of WFPC2 to carry out visual morphological classification of their sample of 20 quasars, and found that more of their radio-quiet objects appeared to be in smooth hosts than in spirals. Although smoothness is not proof of an elliptical, the galaxies are also generally round, unlike the hosts of lower-luminosity quasars imaged with WFPC2 by Hooper, Impey, & Foltz (1997). Boyce et al. (1998) arrived at a similar conclusion for quasars imaged with the WFPC2 PC, based on both morphological and cross-correlation analyses; for the latter, they selected the model that gave the smaller χ^2.

All of the techniques have limitations, and all are based on the possibly faulty premise that hosts are necessarily one type or the other. Nonetheless, we have attempted to discern the galaxy type for the quasars in our (radio-quiet) sample by several methods, the results of which are summarized in Table 4. First, we have examined the images and residual maps for evidence of spiral structure. Although any star-forming regions will admittedly be harder to see in the near-IR than in the visible, we see clear evidence for arms/tidal features in only PG1322+659 and PG1048+342 (which also has a spiral companion), and probably PG0947+396. Second, we have used the profiles in Fig. 4 to determined by inspection which curve in each pair (plotted vs. r or $r^{1/4}$) better approximates a straight line. We have shown various normalizations for the PSF subtraction so the reader can judge the reliability of this technique. Third, we have used the merits from our various 2D fits, where we record the preferred type when the difference in merit is at least 10%. Unfortunately, *even though the galaxy parameters are little affected, the preference for one type over the other depends on the weighting and masking used.* Fourth, we apply the MDK χ^2 test.

One might be tempted on mathematical grounds to trust exclusively the χ^2 statistic used by Taylor et al. (1996) and MDK. Indeed, we find by their method a result similar to theirs, that roughly half of the radio-quiet objects are in deVaucouleurs galaxies. Their criterion for preferring a galaxy type was that $|\chi^2_{deV} - \chi^2_{exp}| > C$, where C is the value of χ^2 that gives 99.99% probability for the number of parameters in the fit. However, for reasons outlined by Jahnke & Wisotzki (2000), this too is problematic. We therefore also consider the latter authors' more conservative χ^2 criterion, namely that a galaxy type is preferred if it cannot be ruled out at 95% confidence, while the alternate model is rejected, say at the 99.9% level (the results are insensitive to the exact level chosen). By this criterion, we make a clean distinction in only *one*

Table 4. Host Galaxy Types[a]

			2D fits			
					χ^2 weight	
ID	Spiral/tidal arms	1D profile	no mask no weight	mask no weight	MDK[b]	JW[c]
PG0026+129	d	d	-	-	e	-
PG0947+396	e?	e	-	e	e	-
PG1048+342	e	d	d	d	d	d
PG1121+422[d]	d	d	-	-	d	-
PG1151+117	d	e	d	-	e	-
PG1322+659	e	-	-	-	d	-
PG1352+183	d	d?	-	e	e	e
PG1354+213	d	d	d	e	d	d
PG1427+480	d	d	d	e	d	-
PG2233+134	d	d	-	-	d	-
MARK876	d	d?	d	e	d	-
UM357	d	d?	-	-	e	-
Q0530-379	d	d	-	-	e	-
NAB1612+26	d	d	-	-	e	-
1628.6+3806	d	d	-	-	e	-
KUV18217+6419	d	d	-	-	-	-

[a]e=exponential, d=deVaucouleurs

[b]χ^2 criterion from McLure, Dunlop, & Kukula (1999)

[c]χ^2 criterion from Jahnke & Wisotzki (2000)

[d]Detection is uncertain

case: PG1352+183 is an exponential. As discussed above, we have likely overestimated the errors in many cases. We therefore also rescale the errors to achieve $\chi^2_\nu = 1$ and repeat the test. This adds to the list PG1048+342, with a deVaucouleurs host, and PG1354+213, with an exponential host. Interestingly, even by the conservative criteria, we find an exponential host with no spiral arms, and a deVaucouleurs host that has arms or tidal features.

Table 4 shows that the methods used by various authors to discriminate the host types give discrepant results, and hints that all such result should be treated with caution. At least in our sample, exponentials and deVaucouleurs models are nearly equally good (or bad) at fitting the 2D images. As the reader can see from Figures 1 and 4, neither model is generally perfect, and the results can be sensitive to the fraction of nuclear light attributed to the galaxy. We note that the methods that down-weight the nuclear region, namely the masked and χ^2 methods, generate a higher fraction of disk systems. One possible explanation is that these are disk galaxies with significant bulge components. When the central regions are neglected, the fit is dominated by the outer, disky components. Unfortunately, with the bulges expected to be comparable to the PSF size, we do not feel we can justify adding a bulge component to the disk fits. However, the facts that arms/tidal features are visible in only two or three of the galaxies, and that all techniques indicate a high fraction of non-disk systems, together *support the notion that many of the radio-quiet quasars live in non-spiral galaxies.*

For completeness, we also examined the distributions of host-galaxy axial ratios b/a. For both exponential and deVaucouleurs models, there is a lack of hosts with low b/a. This is suggestive of an early-type population, but could also be the result of a selection effect. At least for low luminosities, there is a strong bias against finding active nuclei in edge-on spirals, where obscuration in the plane of the host obscures the nucleus (Simcoe et al. 1997).

6.2. Interactions

Interactions have long been suspected of triggering and fueling of quasars, and HST images of nearby quasars have revealed some spectacular examples of hosts with tidal distortions (e.g. Hutchings et al. 1994; Bahcall et al. 1997; Boyce, Disney, & Bleaken 1999; McLure et al. 1999). In our sample, the fraction of hosts that appear to be involved in strong interactions (approximately 4/16) is similar to what has been found in previous studies. However, approximately half of the objects appear to have hosts that are smooth and symmetrical at HST resolution. This is a lower rate than in other studies, though the small numbers make the difference insignificant. For a more detailed discussion of the interaction levels of the quasars from our high-luminosity sample compared to those of low-luminosity quasars, see McLeod & Rieke 1994b.

6.3. Eddington Fractions and the Luminosity/Host-Mass Limit

McLeod & Rieke (1995a), defined a luminosity/host-mass limit for quasar hosts based on a compilation of ground-based near-infrared data. This is not a correlation, as recently misinterpreted by some groups, but rather a limit on the maximum nuclear luminosity possible in a host of a given near-IR luminosity (and presumably mass). From the ground-based data, we found a tight limit well-described by $M_B(nuc) \approx M_H(host)$.

MRS interpret the limit in terms of physical parameters and provide a formula for calculating the fraction of the Eddington luminosity L/L_{edd} at which the quasar radiates. The calculation uses the nuclear B magnitude and the host-galaxy H magnitude along with assumptions about the galaxy mass-to-light ratio, the fraction of the galaxy's mass that resides in the central black hole, and the energy distribution of the nucleus. Under these assumptions, the original $M_B(nuc) \approx M_H(host)$ line translates to a constant Eddington fraction of $\approx 15\%$.

The data for the current project were taken to probe further the luminosity/host-mass limit, and to try intentionally to find galaxies that violate the limit. In Figure 6 we show the host and nuclear magnitudes based on the 1D analysis in this paper. Owing to an updated F160W zero point, more accurate saturation limits, and an improved 1D PSF-subtraction technique, the host magnitudes in the current paper do differ, sometimes substantially, from those in MRS. The zero point accounts for 0.31 mag of the difference. The saturation limit has contributed to a major revision downward of the host magnitude for KUV1821+643, which Percival et al. (2000) noted had an unrealistically luminous host in MRS. The improved 1D technique has corrected a tendency for the host flux to be overestimated in quasars with the lowest ratio of host-to-nuclear light (especially the 6 objects we picked specifically because their hosts had not been detected from the ground, represented by the black pentagons in the Figure).

The magnitudes derived for our sample from HST data make the limit less of a straight line in mag-mag space, but they reinforce the basic result that the most luminous quasars are not found in low-luminosity galaxies. We list in Table 1 the Eddington fractions derived from the current 1D analysis, and note that the results from the 2D deVaucouleurs analyses are similar. The basic MRS conclusion holds, namely that the Eddington fractions are generally $< 20\%$. In fact, the only quasar exceeding this limit in the present study is PG1121+422, with $L/L_{edd} = 0.31$, but our detection of this galaxy is suspect. Its host could be 3 times fainter without crossing the Eddington line.

Recently, Percival et al. (2000) have probed the limit by observing at K the hosts of 14 high-luminosity, radio-quiet quasars. They find that their galaxies lie "to the right of the McLeod & Rieke points" on a plot of nuclear absolute magnitude versus host absolute magnitude, i.e. at higher nuclear luminosity for a given host luminosity than the hosts in our ground-based studies. As shown in Figure 6, some of our quasars do also. Percival et al. (2000) also state that our limit is difficult to transfer quantitatively to their Figure 5 (the PG Survey B magnitudes we used were shown to be systematically too bright by Goldschmidt et al. (1992), but only by ~ 0.3 mag;

the color transformations from R to B and H to K are sensitive to the assumed spectra; etc.). However, we can make an approximate comparison by noting that on the MRS plot, the Eddington line crosses the L^* host galaxy line two nuclear magnitudes brighter than the envelope described by our ground-based limit. This is precisely the region occupied by the Percival et al. (2000) quasars. We conclude that the Percival et al. (2000) quasars also likely are radiating below the Eddington limit, though perhaps closer to it. This is not surprising given that they targeted the most luminous nuclei. Further evidence for consistency with the limit can be seen from their Figure 5, where their quasars overlap with those that McLure et al. (1999) have shown to be sub-Eddington radiators.

A re-statement of the luminosity/host-mass limit based on the physical model is to say that quasars today typically radiate below $\approx 20\%$ of the Eddington rate. Despite choosing quasars that have high nuclear luminosity, and ones for which ground-based attempts to image the hosts had failed, we have not yet found any object that violates the limit corresponding to $L = L_{edd}$. However, we expect such object will be found at higher redshifts according to the predictions of Kauffmann & Haehnelt (2000). Their hierarchical galaxy formation models imply that the massive hosts of today's highest-luminosity quasars formed relatively recently, but that at earlier epochs, luminous quasars will be found in progressively lower-luminosity hosts.

6.4. Notes on Individual Objects

The following notes are based on inspection on an image display of Fig. 1 as well as our full ($20''$) reduced images. The magnitudes of other objects in the fields are simple aperture magnitudes.

PG0026+129 Smooth host with no distortions visible in PSF-subtracted image. A galaxy with $H = 19.2$ is seen at $4\farcs7$ separation, and a faint compact object is at $3\farcs1$.

PG0947+396 Possible broad spiral structure visible in PSF-subtracted image. This may be tidal in origin, due to an interaction with the large edge-on spiral galaxy with $H = 16.65$ seen at $9\farcs9$. If at the redshift of the quasar, this spiral is at a projected separation of 28 kpc. A second galaxy with $H = 18.7$ is at $5\farcs0$.

PG1048+342 Spiral structure visible in PSF-subracted image, but the 1D profile indicates a deVaucouleurs profile. As with PG0947, the structure could be tidal in origin, due to interaction with the large spiral ($H = 17.3$, and similar in size to the quasar host) at a projected separation of $3\farcs4$ (8.2 kpc if at the quasar's redshift). This galaxy appears to be part of a group. Besides the large spiral, there are at least 5 fainter spirals and distorted galaxies within $18''$.

PG1121+422 No host is visible on the images, but the 1D profile suggests that a compact one is present.

PG1151+117 Smooth host is visible on the PSF-subtracted image. DeVaucouleurs fit residual shows an elongated structure right-left (north-south). An $H = 18.8$ galaxy is at $3\farcs6$, and a faint point source is roughly twice that far away.

PG1322+659 Beautiful 2 armed spiral host with bar-like structure right-left (north-south). Several galaxies, including one that is likely similar in size to the host, are visible on the edge of our full frame at $\sim 10''$. If at the redshift of the quasar, the large galaxy is at a projected separation of 24 kpc and could be responsible for the host's broad arms.

PG1352+183 Smooth host. A faint ($H = 21$), elongated galaxy is seen at $5\farcs2$.

PG1354+213 Smooth host.

PG1427+480 Smooth host. An $H = 19.6$ galaxy is at $3\farcs1$.

PG2233+134 Smooth host. There are two small galaxies in our full frame: $H = 20.6$ at $3\farcs6$, $H = 19.6$ at $9\farcs7$.

MARK876 [Also called PG1613+658] Severely distorted host. The host galaxy filled so much of the frame that removal of the NICMOS quadrant effect was problematic. As a result, the frame is not as flat as for the other objects. However, the nearly triangular outer contours with a straight left edge is not an artifact, but is also visible on ground-based images. What the NICMOS image reveals is that a companion, with $H = 16$ and at a projected separation of $2\farcs2$ (4.3 kpc), is appears to be embedded within the host. The PSF-subtracted image shows large-scale, asymmetric, tidal features that probably resulted from this interaction.

UM357 Host is very compact, and too small for structure to be visible.

Q0530-379 Smooth host. There are several other galaxies visible in the full frame: $H = 19.4$ at $4\farcs2$, $H = 19.8$ at $6\farcs5$, $H = 18.3$ at $8\farcs7$, and $H = 20.6$ at $9\farcs7$.

NAB1612+26 Host is compact but clearly elongated left-right (northwest-southeast). Two diffuse, faint galaxies are visible in our full frame: $H = 18.8$ at $6\farcs0$, and $H = 21.6$ at $9\farcs2$.

1628.6+3806 PSF-subtracted image shows asymmetric extension to lower left (northeast). There are two small galaxies in the frame: $H = 19.3$ at $3\farcs5$, and $H = 20.5$ at $5\farcs6$. There is also a star at $5\farcs6$.

KUV18217+6419 1D profile shows that this is clearly a deVaucouleurs host, yet deVaucouleurs fits converged only when masked. This is perhaps due to interference from a linear feature extending up (southwest) from the host. However, it is also possible that the extremely high nuclear brightness has compromised the fitting; it has by far the brightest nucleus in our sample, and the host-to-nucleus flux ratio is low. Still, the galaxy is intrinsically the most luminous in our sample. There are two galaxies at $9\farcs5$ ($H = 17.3,\ 17.6$) seen on opposite sides of the quasar in our full frame.

7. Conclusions

We have imaged 16 low-redshift, high-luminosity quasars with NICMOS. Using stellar images as PSFs has worked extremely well, and NICMOS has done a superb job of showing the host galaxies with high contrast against the bright nucleus. We find the following results.

(i) For redshifts $z \lesssim 0.3$, the host-galaxy magnitudes derived from ground-based data using our 1D analysis technique are very reliable (within ~ 0.30 mag) unless there are companions that cannot be resolved. Therefore, general conclusions about host luminosities from our previous papers should be robust.

(ii) Distinguishing between deVaucouleurs and exponential hosts based on various fitting techniques is questionable, especially given that neither law is likely perfect. For 2D fits, we recommend a very conservative χ^2 criterion for discrimination. While some previously used methods appear to distinguish between types in almost every case, they are often at odds with the more conservative criterion, which can distinguish between types in only ~ 3 cases out of 16. The 1D radial profiles are also very useful. Fortunately, HST allows us to look directly for spiral arms and other morphological features in the hosts. We concur with previous studies that have found radio-quiet quasars often live in deVaucouleurs hosts.

(iii) Approximately 4 of the 16 hosts are undergoing strong interactions with companions. However, nearly half of the hosts are smooth and symmetric, a reminder that current-epoch interactions are not a necessary condition of quasar activity.

(iv) Assuming that galaxies contain central black holes with 0.6% of the galaxy's mass (see MRS for details), 15 of the 16 quasars in our sample radiate at $\sim 2 - 20\%$ of the Eddington rate. Our host detection for PG1121+422 is uncertain, so its rate of 31% Eddington may be a lower limit. Despite intentionally choosing high-luminosity quasars whose hosts were hard to detect from the ground, we have failed to find any object that violates a luminosity/host-mass limit corresponding to $L = L_{Edd}$.

Thanks to George Rieke and Lisa Storrie-Lombardi for their work on the HST proposal and MRS, and to Lisa also for especially valuable comments on this paper. We thank the NICMOS team for putting such a superb instrument in orbit, Erin Condy for help with the data reduction, Ray Weymann for helpful ideas during the course of this project, and Marcia Rieke for the calibration files used with *nicred*_1.8. We thank the anonymous referee for comments that helped us to improve the presentation significantly. Support for this work was provided by NASA through grant number GO-07421.01-96A from the Space Telescope Science Institute, which is operated by the Association of Universities for Research in Astronomy, Inc., under NASA contract NAS5-26555. We also gratefully acknowledge support from the Keck Northeast Astronomy Consortium.

REFERENCES

Bahcall, J. N., Kirhakos, S., Saxe, D. H., & Schneider, D. P. 1997, ApJ, 497, 642

Boyce, P. J., et al. 1998, MNRAS, 298, 121

Boyce, P. J., Disney, M. J., & Bleaken, D. G. 1999, MNRAS, 302, L39

Cristiani, S., & Vio, R. 1990, A&A, 227, 385

Goldschmidt, P., Miller, L., LaFranca, F., & Christiani, S. 1992, MNRAS, 256, 65P

Hooper, E. J., Impey, C. D., & Foltz, C. B. 1997, ApJ, 480, 95

Hutchings, J. B., Holtzman, J., Sparks, W. B., Morris, S. C., Hanisch, R. J., & Mo, J. 1994, ApJ, 429, L1

Hutchings, J. B. 1995, Nature, 376, 118

Jahnke, K., & Wisotzki, L. 2000, MNRAS, submitted

Kauffmann, G., & Haehnelt, M, 2000, MNRAS, 311, 576

Lehár, J., et al. 2000, ApJ, 536, 584

McLeod, B. A., in The 1997 HST Calibration Workshop with a new generation of instruments, Baltimore, MD, ed. S. Casertano, R. Jedrzejewski, C. D. Keyes, & M. Stevens, (Baltimore, MD: STScI) p. 281

McLeod, K. K., & Rieke, G. H. 1994a, ApJ, 420, 58

McLeod, K. K., & Rieke, G. H. 1994b, ApJ, 431, 137

McLeod, K. K., & Rieke, G. H. 1995a, ApJ, 441, 96

McLeod, K. K., & Rieke, G. H. 1995b, ApJ, 454, L77

McLeod, K. K., Rieke,G. H., & Storrie-Lombardi, L. J. 1999, ApJ, 511, L67 (MRS)

McLure, R. J., Kukula, M. J., Dunlop, J. S., Baum, S. A., O'Dea, C. P., Hughes, D. H. 1999, MNRAS, 308, 377

McLure, R. J., Dunlop, J. S., & Kukula, M. J. 1999, astro-ph/9912044

Percival, W. J., Miller, L., McLure, R. J., & Dunlop, J. S. 2000, astro-ph/2002199

Rönnback, J., van Groningen, E., Wanders, I., & Örndahl, E. 1996, MNRAS, 283, 282

Simcoe, R., McLeod, K. K., Schachter, J., & Elvis, M. 1997, ApJ, 489, 615

Taylor, G. L., Dunlop, J. S., Hughes, D. H., & Robson, E. I. 1996, MNRAS, 283, 930

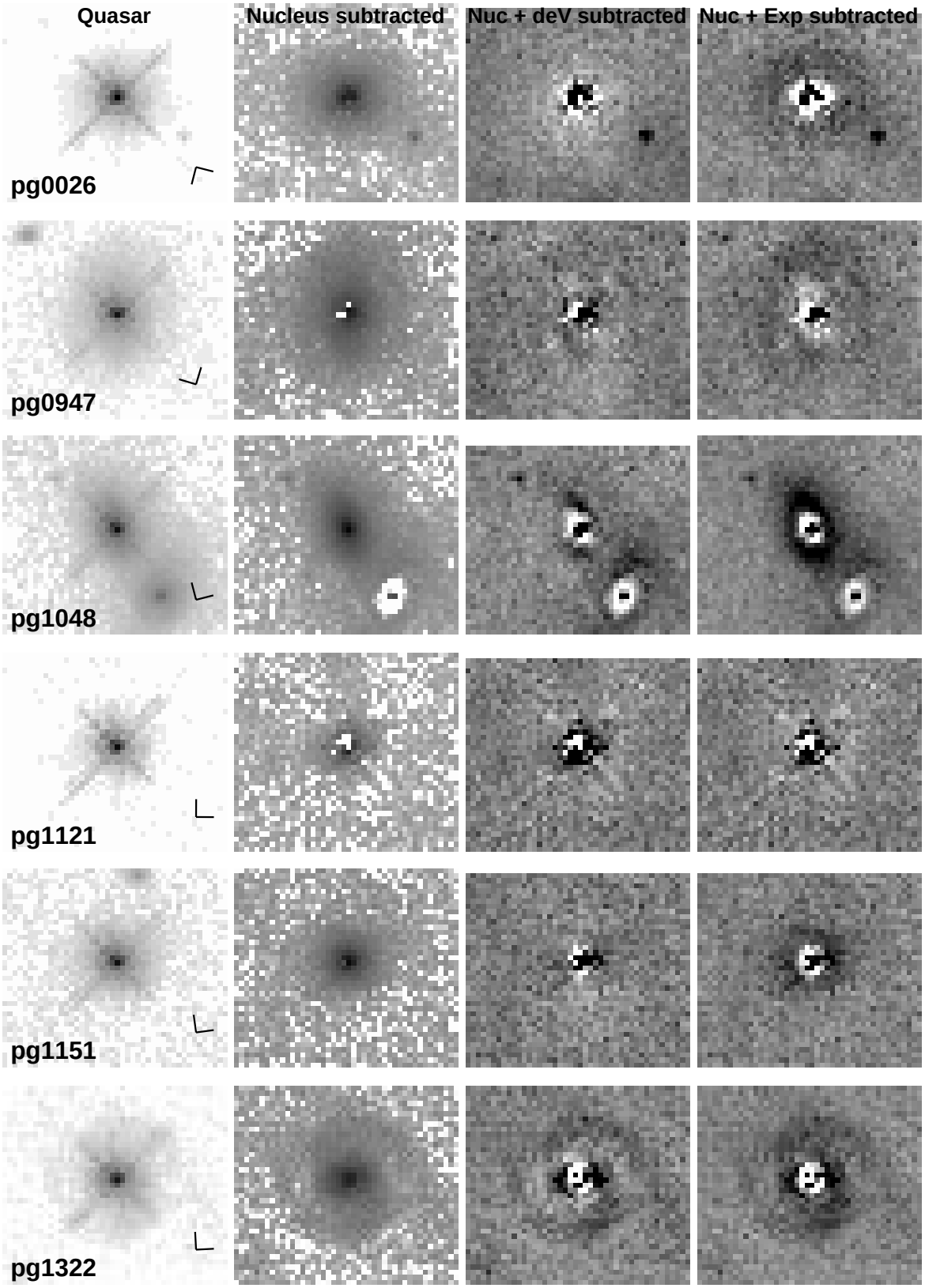

Fig. 1.— Central 9.″6 of the quasar images on a logarithmic greyscale stretch. Angle marker shows North and East (counterclockwise from N). From left to right, the columns are: (a) quasar; (b) quasar with nucleus removed based on deVaucouleurs law fit (for KUV18217+6419 we show the exponential law fit because no unmasked deVaucouleurs model converged); (c) quasar with nucleus and deVaucouleur model removed; (d) quasar with nucleus and exponential model removed. Columns (b)-(d) were generated from unweighted fits using PSF0026.

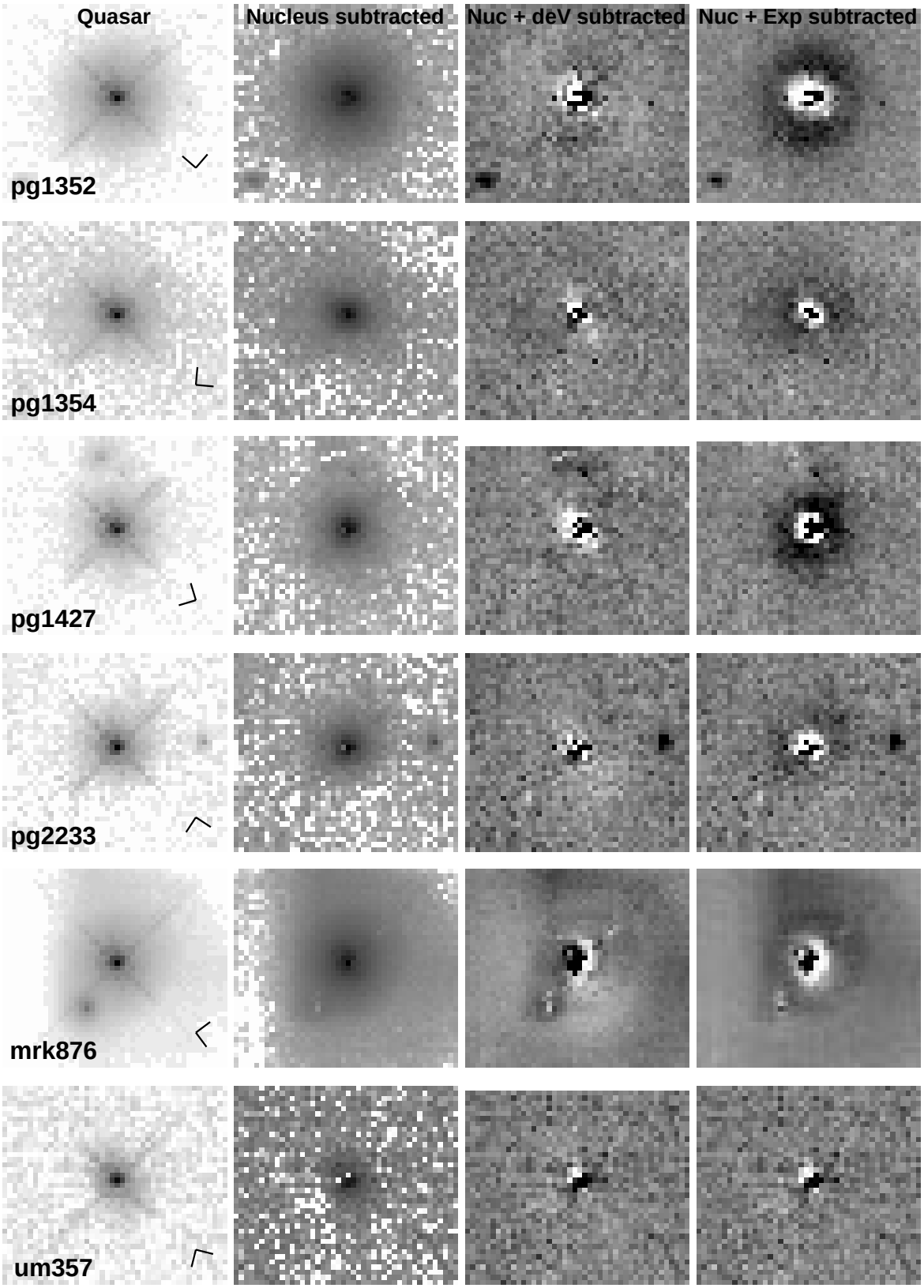
Quasar
Nucleus subtracted
Nuc + deV subtracted
Nuc + Exp subtracted
pg1352
pg1354
pg1427
pg2233
mrk876
um357

Fig. 1. — cont'd

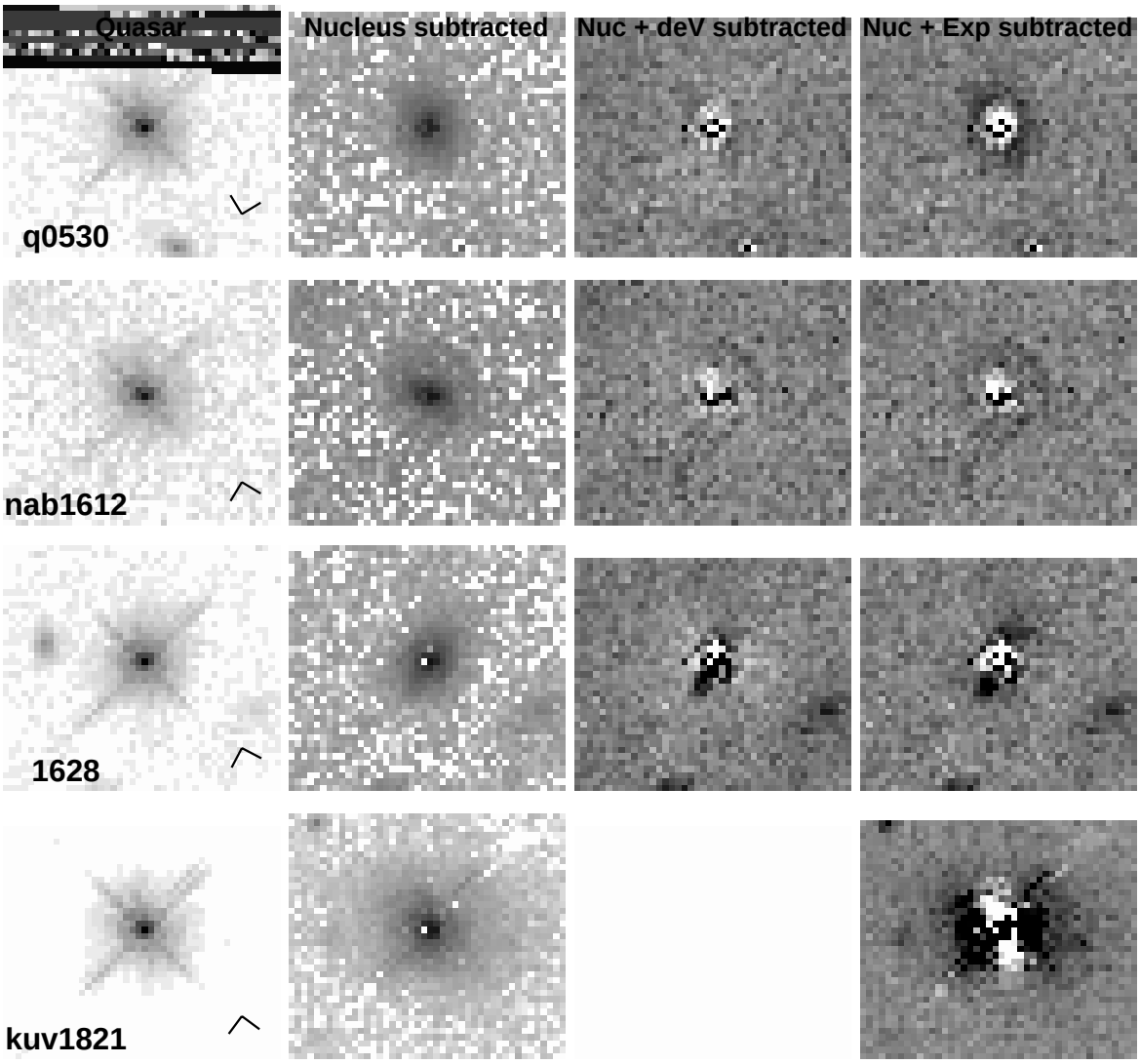
Quasar
Nucleus subtracted
Nuc + deV subtracted
Nuc + Exp subtracted
q0530
nab1612
1628
kuv1821

Fig. 1. — cont'd

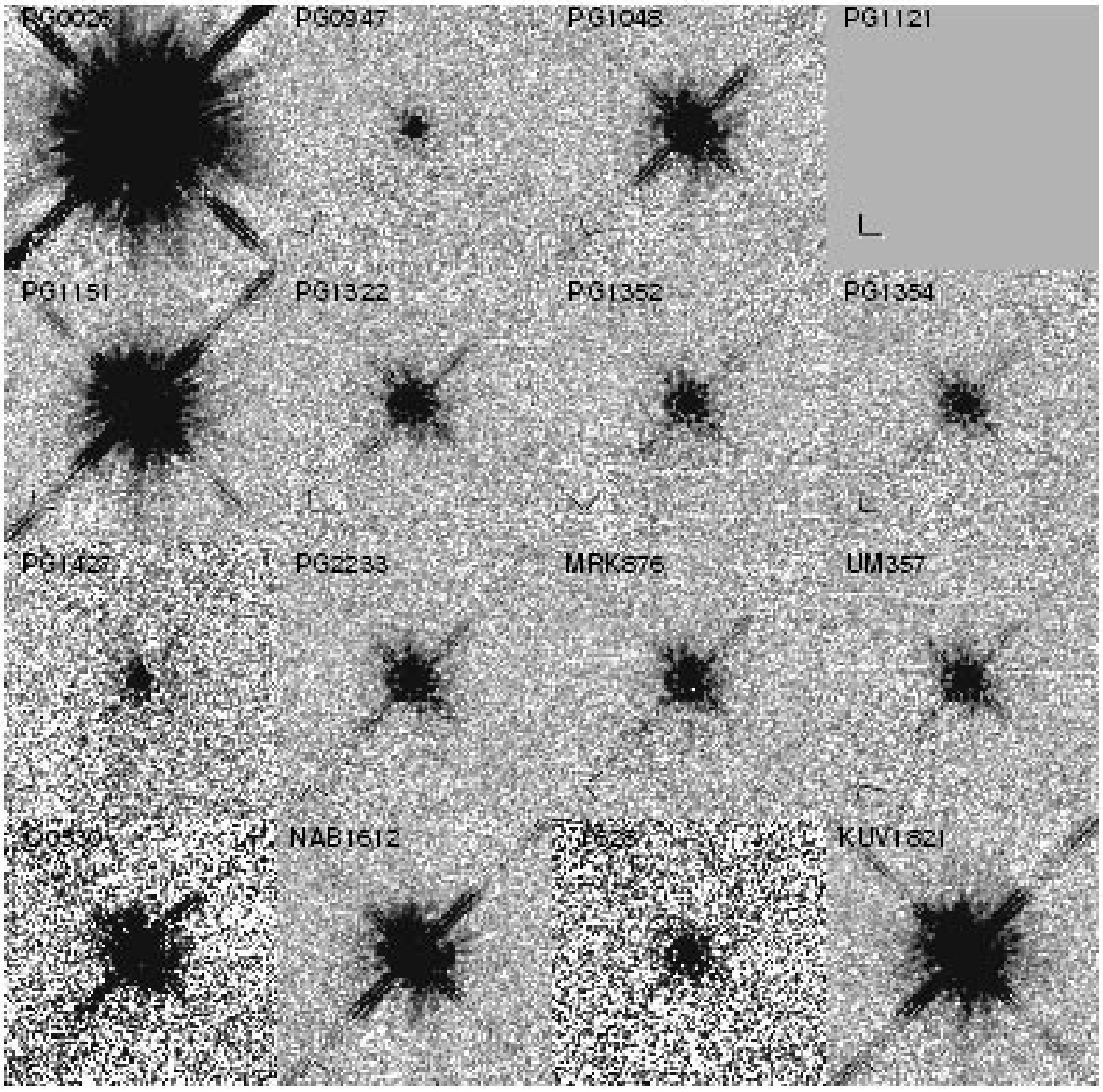

Fig. 2.— Images of the PSF stars on a logarithmic greyscale stretch. Same angular scale and orientations as in Fig. 1.

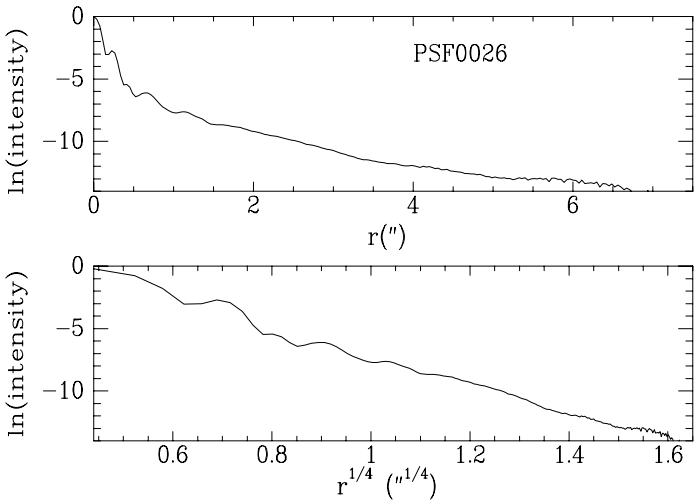

Fig. 3.— Full 1D radial profile of the brightest PSF in our sample, PSF0026. Profiles are shown versus r (top plot) and $r^{1/4}$ for comparison with quasar profiles in Fig. 4.

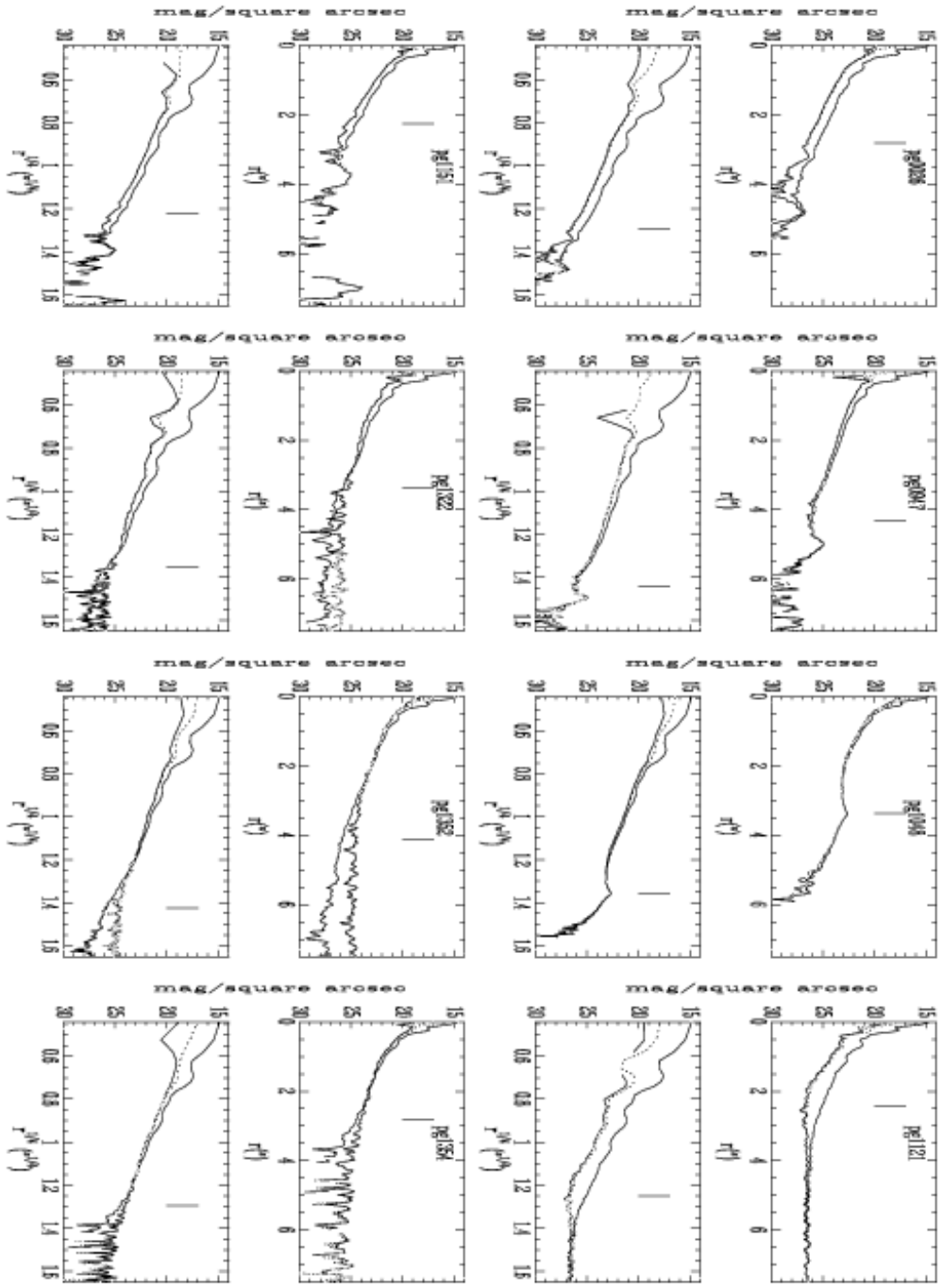

Fig. 4.— 1D radial profiles of the quasars versus r (top plot in each pair) and $r^{1/4}$. The three curves on each plot show different PSF subtractions: none (top solid line), 100% (bottom solid line), and just monotonic as described in the text (dotted line). The vertical line shows the radius to which the profile was integrated for computation of the host-galaxy magnitude. Outside of this line, the profile is compromised by either a companion or noise. Pure exponential disks (with no bulge component) would appear as straight lines versus r,, whereas deVaucouleurs galaxies would appear as straight lines versus $r^{1/4}$.

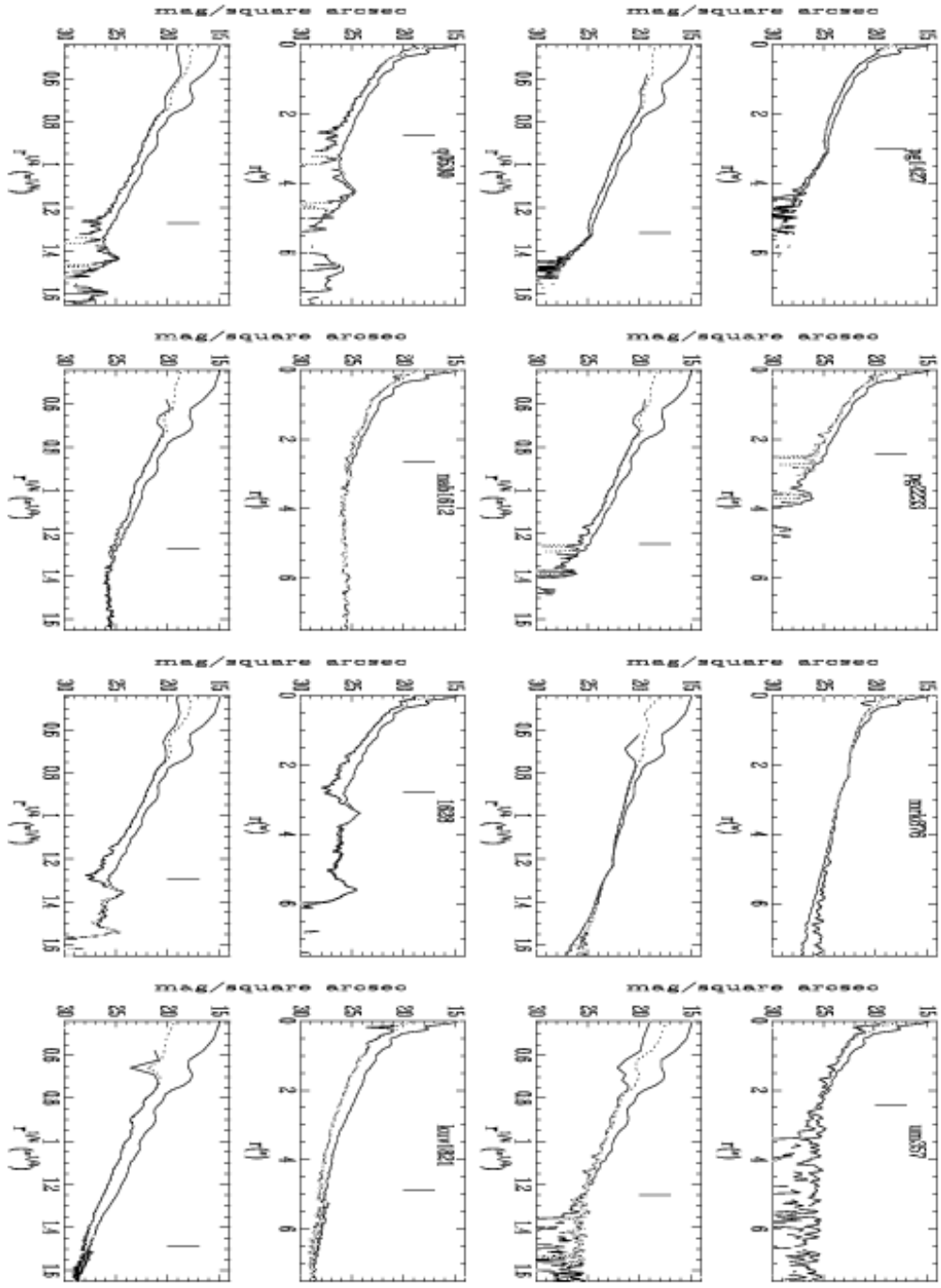
mag/square arcsec
mag/square arcsec
mag/square arcsec
mag/square arcsec
mag/square arcsec
mag/square arcsec
mag/square arcsec
mag/square arcsec

Fig. 4. — cont'd

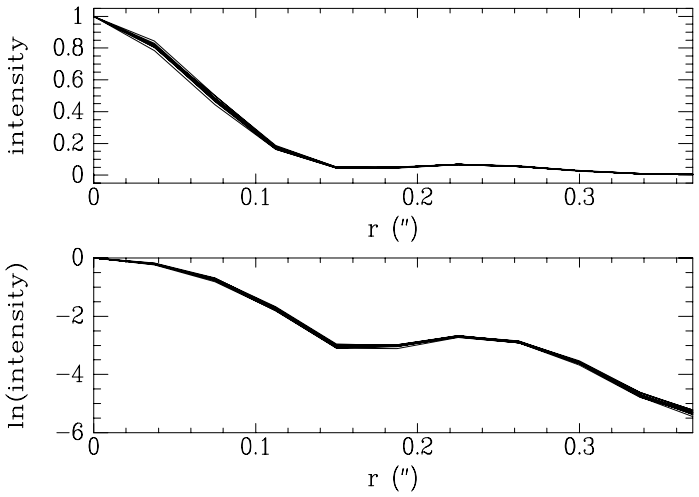

Fig. 5.— Central parts of the 1D radial profiles of all 15 PSF stars, normalized by central intensity. Profiles are shown with both linear (top) and natural log scaling to highlight differences at different radii. Spreading at large radii is due to noise in the fainter PSF stars.

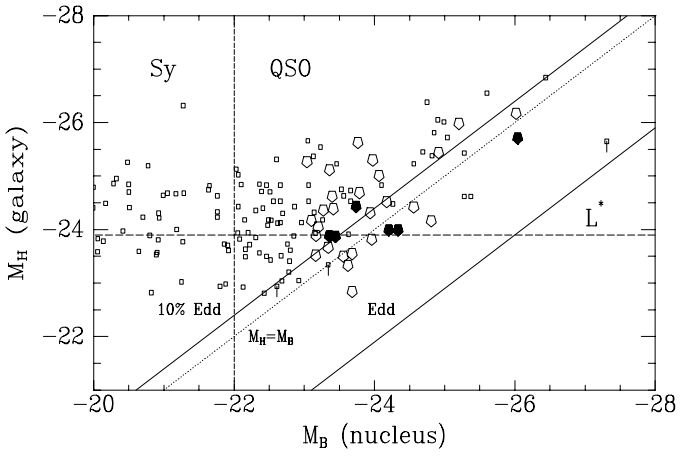

Fig. 6.— Galaxy versus nuclear absolute magnitudes for QSOs. Low-redshift QSOs and Seyferts shown as boxes are taken from MRS and references therein. QSOs shown as open pentagons constitute the high-luminosity sample from McLeod & Rieke 1994b, with host magnitudes derived from either NICMOS images (this paper) or WFPC2 images (Bahcall et al. 1997; McLure et al. 1999). Filled pentagons are the other 6 QSOs from our NICMOS imaging. Also shown are the QSO/Sy boundary (dashed vertical line), position of an L^* galaxy (dashed horizontal line), and loci of Eddington and 10% Eddington luminosities. The original "luminosity/host-mass limit" is shown by dotted line for reference.